Check for updates

Received: 24 July 2022 | Revised: 17 April 2023 | Accepted: 21 April 2023

DOI: 10.1002/cey2.409

RESEARCH ARTICLE

CARBON ENERGY WILEY

Single-atom Pt on carbon nanotubes for selective electrocatalysis

Samuel S. Hardisty[1] | **Xiaoqian Lin**[2] | **Anthony R. J. Kucernak**[2] | **David Zitoun**[1]

[1]Department of Chemistry, Bar Ilan Institute of Nanotechnology and Advanced Materials (BINA), Bar Ilan University, Ramat Gan, Israel

[2]Department of Chemistry, Molecular Science Research Hub, Imperial College London, London, UK

Correspondence
David Zitoun, Department of Chemistry, Bar Ilan Institute of Nanotechnology and Advanced Materials (BINA), Bar Ilan University, Ramat Gan 5290002, Israel.
Email: david.zitoun@biu.ac.il

Funding information
H2020 Marie Sklodowska-Curie Actions, Grant/Award Number: FLOWCAMP; Wohl Foundation for Research for the Promotion of UK-Israel Research Cooperation; Israel Ministry of Energy, Grant/Award Number: 220-11-047

Abstract

Utilizing supported single atoms as catalysts presents an opportunity to reduce the usage of critical raw materials such as platinum, which are essential for electrochemical reactions such as hydrogen oxidation reaction (HOR). Herein, we describe the synthesis of a Pt single electrocatalyst inside single-walled carbon nanotubes (SWCNTs) via a redox reaction. Characterizations via electron microscopy, X-ray photoelectron microscopy, and X-ray absorption spectroscopy show the single-atom nature of the Pt. The electrochemical behavior of the sample to hydrogen and oxygen was investigated using the advanced floating electrode technique, which minimizes mass transport limitations and gives a thorough insight into the activity of the electrocatalyst. The single-atom samples showed higher HOR activity than state-of-the-art 30% Pt/C while almost no oxygen reduction reaction activity in the proton exchange membrane fuel cell operating range. The selective activity toward HOR arose as the main fingerprint of the catalyst confinement in the SWCNTs.

KEYWORDS
confinement, electrocatalysis, hydrogen, platinum, single atom catalysts

1 | INTRODUCTION

A huge range of applications exist for platinum group metal (PGM) catalysts. In electrocatalysis, they are highly favored due to high activity and stability in both acid and alkaline electrolytes for the hydrogen oxidation reaction (HOR),[1,2] hydrogen evolution reaction (HER),[3,4] oxygen reduction reaction (ORR),[5] and oxygen evolution reaction (OER)[6] among others. This means that technologies that depend on these reactions, such as energy conversion systems such as proton exchange membrane fuel cell (PEMFC) and water electrolyzers, and also rely on PGM. These applications produce pressure on the supply of PGM, which is already incredibly scarce.[7] This pressure results in worries about a stable supply as more technologies are deployed using PGM, such as the replacement of fossil fuel automobiles with PEMFC-powered vehicles and the water electrolyzers required to produce hydrogen to power them. Even with this pressure, it is widely accepted that only 40% of the Pt in a PEMFC electrode is active, a clear inefficiency that must be resolved before the technology can be considered sustainable.[8–10] By reducing the size of the PGM nanoparticles down to single, isolated atoms, very high utilization of

This is an open-access article under the terms of the Creative Commons Attribution License, which permits use, distribution, and reproduction in any medium, provided the original work is properly cited.
© 2023 The Authors. *Carbon Energy* published by Wenzhou University and John Wiley & Sons Australia, Ltd.

the catalyst material can be achieved, maximizing the activity while minimizing the required loading.[11]

Since the terms' inception in 2011,[12] examples of single-atom catalysts (SACs) have been published for nearly every metal.[13] This hotbed of research seeks to form stable SACs that do not agglomerate to form nanoparticles, which require a strong interaction of the atoms with the support. Metal oxides, such as ceria[14] or titania,[15,16] are common supports due to their strong interaction with metal atoms deposited on their surface. In the field of electrocatalysis, however, the support must be highly electronically conductive to facilitating electron transport from the catalyst to the attached electrical system. This disqualifies a vast swath of these oxide supports. Suitable supports for single-atom electrocatalysts that have been found so far include graphene,[17] nitrogen-doped carbons,[18] MXenes,[19] and carbon nanotubes.[20]

The majority of research has focused on reactions such as HER and ORR, and little has been published about HOR.[21] Only one article with experimental data could be found, which used covalent triazine frameworks to support Pt SAC for selective HOR over the ORR.[22] Further development of SAC for HOR would allow the reduction in costs and use of critical materials for technologies that rely on the reaction, such as PEMFCs, as well as uncover selectivity toward the reaction that could be advantageous.

In this work, we report a single-atom Pt catalyst, synthesized through a redox process taking place inside SWCNTs. The catalyst showed good activity for HOR, whilst minimizing ORR. The Pt SAC also showed superior stability over a commercial Pt nanoparticle catalyst.

2 | EXPERIMENTAL SECTION

2.1 | Synthesis

Single-wall carbon nantubes (SWCNTs) (Tuball™) were purchased from OCSiAl, with an average diameter of 1.6 nm and length >5 μm. The as-received SWCNTs (ar-SWCNT) were first oxidized in a H_2SO_4:HNO_3 (1:3) mixture for 4 h, then washed with deionized (DI) H_2O (Merck Millipore Milli-Q, 18.2 MΩ cm TOC < 10 ppb) until the filtrate was pH 7, and dried producing opened SWCNTs. These SWCNTs were then dried under vacuum (130 mbar) for 4 h, and 1.32 mL of 16 mg mL^{-1} K_2PtCl_4 solution was introduced to 100 mg of them whilst the vessel was evacuated. The vessel was then sonicated for 5 min, before being opened to the atmosphere and stirred for 1 h (SA8) or 14 h (SA24). The samples were then dried under vacuum and washed with DI H_2O, with repeated vacuum drying steps between each wash. 100 mg of SA24 was sintered at 700°C under Ar flow for 2 h to form NP24.

2.2 | Structural characterization

High-resolution transmission electron microscopy (HRTEM) observation was performed with a JEOL JEM-2100 operated at 200 kV. High-angle annular dark field scanning transmission electron microscopy (HAADF-STEM) was taken on an FEI TITAN transmission electron microscope (TEM) operated at 300 kV. The samples were deposited on Cu grids with lacey carbon from an isopropanol dispersion. XRD was performed with a Brucker D8 Advanced X-Ray diffractometer, using Cu Kα radiation. X-ray photoelectron spectroscopy (XPS) was conducted using a Nexsa X-ray photoelectron spectrometer system (Thermo Fisher Scientific) with a monochromated Al Kα X-ray source. Measurements were taken at room temperature, under a high vacuum ($<3.0 \times 10^{-9}$ Torr). A 400 μm spot size was used, with a pass energy of 50 eV.

The amount of metal was assessed via ashing of the samples at 1073 K, followed by the dissolving of the ash with aqua regia and ICP-AES (Ultima-2 spectrometer; JobinYvon Horiba) of the resulting solution.

2.3 | Electrochemical characterization

The process of making the floating electrodes (FE) and the electrochemical measurements followed the protocols reported,[23] and it is briefly mentioned here. For each catalyst, 2 mg of solid catalyst was suspended in 4 mL of 1:1 isopropanol (VWR, AnalaR NORMAPUR) to DI water and sonicated (BANDELIN SONOCOOL) on full power (35 kHz, 100%) at 288 K until a homogeneous ink was obtained. Before making the FEs, the ink was diluted corresponding to the desired catalyst loading on the electrode. The FE was made by vacuum filtrating 100 μL of the diluted ink onto a gold-coated track-etched polycarbonate (Sterlitech, 0.4 μm pore size, 47 mm, PCTF0447100) and further made hydrophobic by drop-casting 0.1 μL of 1 wt.% Teflon AF 2400 (DuPont) solution in Fluorinert FC-40 (Sigma-Aldrich) on the non-coated side of the substrate. The electrochemical "break-in" was achieved using the same protocols developed for measuring Pt/C catalysts. Cyclic voltammograms were performed under hydrogen and oxygen in turn until the performance of the electrode became stable. After all the electrochemical measurements were finished, the electrodes were digested in aqua regia; their

26379368, 2024, 1, Downloaded from https://onlinelibrary.wiley.com/doi/10.1002/cey2.409 by Imperial College London, Wiley Online Library on [07/03/2024]. See the Terms and Conditions (https://onlinelibrary.wiley.com/terms-and-conditions) on Wiley Online Library for rules of use; OA articles are governed by the applicable Creative Commons License

loadings were determined with ICP-MS (Agilent 8900 ICP-QQQ), and the residual membrane was checked for full Pt dissolution via XPS. The mass current density (or activity) is the measured current normalized by the mass of Pt detected from the ICP-MS.

3 | RESULTS AND DISCUSSION

To produce Pt single-atom and nanoparticle samples, SWCNTs were opened using an established procedure that minimizes defect formation in the SWCNTs. A K_2PtCl_4 solution was introduced to the opened SWCNTs in an evacuated vessel, forcing the solution into the internal pores of the SWCNTs through capillary forces. Within the SWCNT, the Pt^{2+} is reduced to Pt^0 to form single atoms without additional reducing agents, as we will discuss below. After 1 or 14 h, the samples were then dried under a vacuum. All samples were repeatedly washed with DI water and dried under vacuum, and some of the 14-h impregnation samples were then sintered at 700°C under Ar to form nanoparticles. Inductively coupled plasma atomic emission spectroscopy (ICP-AES) showed that the single-atom samples had 8 wt.% Pt (SA8) after 1 h of impregnation time and 24 wt.% Pt (SA24) after 14 h of impregnation time, whilst the nanoparticle sample had 24 wt.% Pt (NP24).

Aberration-corrected STEM in HAADF mode was used to analyze the morphology of the samples (Figures 1A,D and S1). The micrographs show clearly single-atom Pt dispersed throughout the SWCNT network in both SA8 and SA24. In Figure 1B, atomic resolution energy-dispersive X-ray spectroscopy (EDX) confirms that the atomic species that can be seen is Pt. Although some larger species are present, this can be explained by the 3D nature of the nanotube and the two-dimensional (2D) nature of the micrographs. Interestingly, the O mapping (Figure 1C) shows a correlation with the Pt, suggesting that O inclusion into the SWCNT is related to the Pt single-atom deposition. The higher magnification micrograph of SA8 (Figure 1D) shows that the dispersion of the single atoms follows the internal pores of the SWCNTs, indicating that they are confined within. A profile drawn over three different groups of atoms (Figure 1E) gives multiple peaks with full width at half maximum (FWHM) around 0.17 nm, matching the atomic diameter of Pt atoms (170 pm). This clearly demonstrates the single-atom nature of the Pt within these samples. The annealed sample (NP24) shows nanoparticles and nanorods within the SWCNTs, with a particle width distribution matching the width distribution of the SWCNTs (Figure S2) as measured via TEM. The confined nanoparticles formed after sintering clearly demonstrate that the single atoms are inside the SWCNTs. This material has been characterized in-depth in another publication.[24]

XPS was used to assess the chemical nature of the samples. The XPS has been recorded on nanoparticles (NP24) and we used the formalism commonly found in the investigation of nanoparticle to fit the data set: bulk refers to the core atoms with a zerovalent state, surface to the surface atoms with lower coordination state (oxidation state between 0 and 2), and Pt-O to Pt(II) oxidation state. The classic Pt 4f XPS spectrum was recorded for the NP24 sample, split into three components of the bulk, the surface atoms, and oxidized Pt species, with the Pt $4f_{7/2}$ peaks centered at 71.7, 73.1, and 74.7 eV.[25] The two single-atom samples only show two species, giving Pt $4f_{7/2}$ peaks centered at 72.5 eV and at 74.6 eV, respectively, for Pt(0) and Pt(II). There was no peak corresponding to the higher oxidation state Pt(IV). The higher binding energy peaks are evidently caused by oxidized Pt species, Pt^{2+}, and account for 13% and 11% of the total Pt for SA8 and SA24 respectively and 12% for NP24. This indicates that the oxidized species are Pt atoms that have adsorbed oxygen, rather than remaining unreduced Pt from the synthesis, as the amount is consistent across the samples. The other Pt $4f_{7/2}$ peak is a signature of the single atoms, indicating that they have a partial positive charge due to the increased binding energy, presumably due to charge transfer between the Pt and the SWCNT. This shift has been shown before for single-atom Pt catalysts.[26] The N 1s spectra of the SA and empty SWCNTs (Figure S3) show that there is no nitrogen detectable in the sample, confirming that it is C bonding to the Pt SAs.

The C 1s and O 1s spectra of the samples, alongside the SWCNTs before impregnation, were fit according to standard fitting procedures for SWCNTs (Figure S4). The relative quantities of the C–O, C═O, COO, and the SWCNT π–π^* transition peaks from the C 1s and O–C and O═C peaks from the O 1s spectra are shown in Figure 2B. We can see that after impregnation, the SWCNT is oxidized, with increasing amounts of C–O and C═O species in both C 1s and O 1s spectra. This corresponds to a small decrease in the π–π^* transition peak, indicating an increase in defects in the SWCNT structure. These changes increase as the $PtCl_4^{2-}$ is left inside the SWCNTs for a longer time to form SA24. Upon annealing, the C═O and COO species decrease, whilst the π–π^* transition peak increases above its initial value, showing that annealing removes have more defects than just those formed during the synthesis. The C–O species stay the same according to the O 1s spectrum, whilst that of C 1s shows a slight decrease (Figure 2B). This indicates that these species are relatively stable after the deposition of the Pt and that Pt is possibly bonded to them.

26379368, 2024, 1, Downloaded from https://onlinelibrary.wiley.com/doi/10.1002/cey2.409 by Imperial College London, Wiley Online Library on [07/03/2024]. See the Terms and Conditions (https://onlinelibrary.wiley.com/terms-and-conditions) on Wiley Online Library for rules of use; OA articles are governed by the applicable Creative Commons License

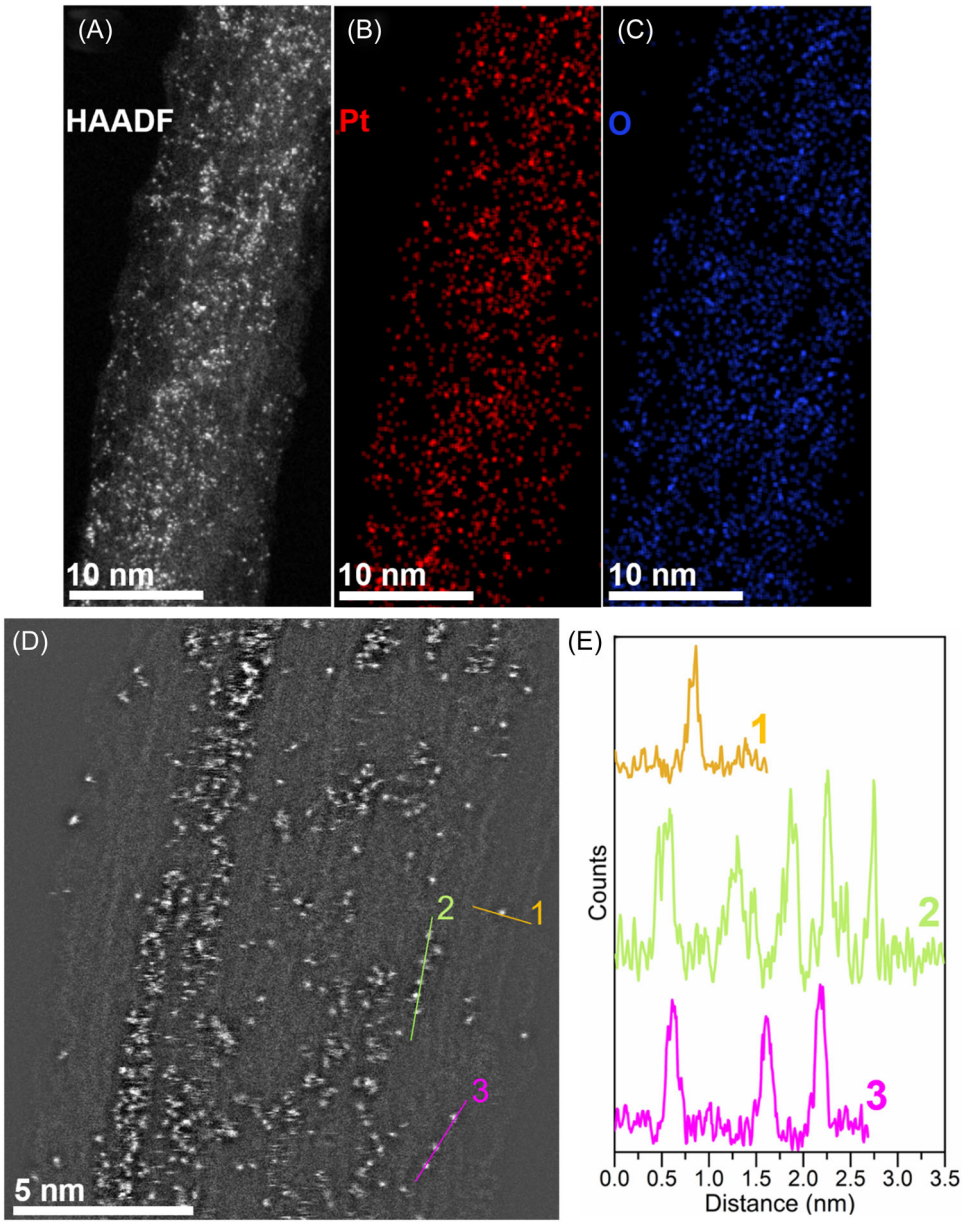


FIGURE 1 HAADF-STEM micrographs of (A) SA24 with EDX (B) Pt and (C) O mapping, and (D) SA8 with (E) corresponding line profiles.

The survey spectrum (Figure S4) reveals the presence of Cl with a ratio Pt:Cl of 0.7:1, which are leftovers from the precursor. We cannot assess with certainty the nature of the chloride species. A reasonable hypothesis would be that the chloride still binds the Pt atoms, which could explain the presence of Pt(II) as shown in the XPS spectrum. Therefore, the sample would consist of Pt(0) single atoms and Pt(II)-Cl_2 species.

X-ray absorption spectroscopy was conducted to study the electronic and atomic environment of the Pt in the samples. The X-ray absorption near edge structure (XANES) of the Pt L_3-edge samples, compared with Pt foil, are shown in Figure 2C. The XANES show a white line, a well-known feature of Pt XANES just above the L_3-edge absorption edge resulting from a dipole transition from Pt $2p_{3/2}$ and $2p_{1/2}$ to the $5d_{5/2,3/2,}$ and $5d_{3/2}$ bands. The intensity of the white line for the SA8, SA24, and NP24 samples is substantially higher than that of Pt foil, indicating a higher unoccupied density of states of $5d_{5/2}$ and $5d_{3/2}$ character. The SA24 and NP24 samples have roughly the same intensity, whilst the SA8 white line is higher, indicating a decrease in the electrons in the d orbital. The negative shift in E_0 shows that this is not due to oxidation and that the species are close to being zerovalent.

26379368, 2024, 1, Downloaded from https://onlinelibrary.wiley.com/doi/10.1002/cey2.409 by Imperial College London, Wiley Online Library on [07/03/2024]. See the Terms and Conditions (https://onlinelibrary.wiley.com/terms-and-conditions) on Wiley Online Library for rules of use; OA articles are governed by the applicable Creative Commons License

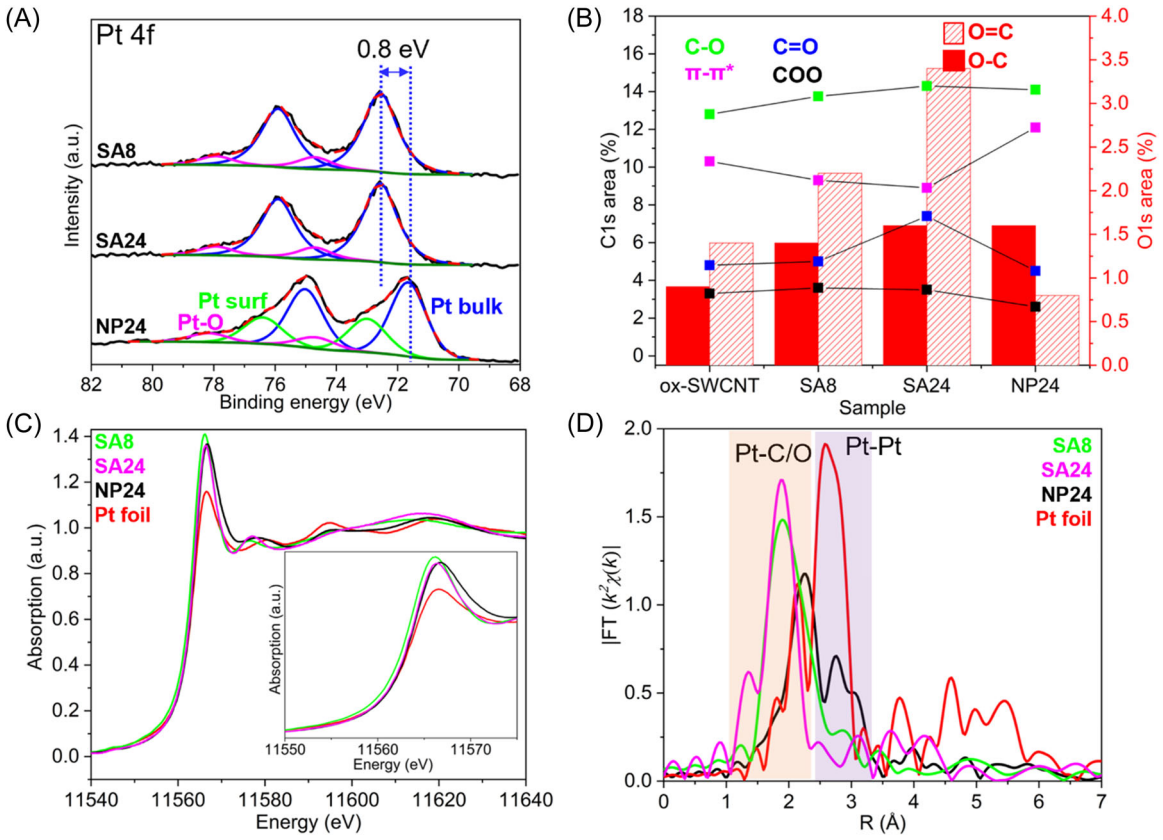


FIGURE 2 (A) Pt 4f and (B) quantities of the fitted C 1s and O 1s XPS spectra of empty SWCNTs, SA8, SA24 and NP24, (C) normalized XANES at the Pt L_3 edge, and (D) K^3 weighted Fourier transform of the EXAFS of SA8, SA24, NP24, and Pt foil.

The Fourier transforms of the extended X-ray absorption fine structure (EXAFS) are shown in Figure 2D. The oscillations of the EXAFS region are caused by the scattering of ejected photoelectrons from neighboring atoms, and the Fourier transform of this gives an indication of the local atomic environment surrounding the species. The EXAFS of Pt foil and NP24 show two distinctive regions, with the peak at 2.0 Å being caused by Pt bonding to lighter atoms such as O and C (and possibly Cl), whilst the peak at around 2.6 Å is caused by Pt-Pt bonding. Unfortunately bonding with C and O are indistinguishable due to similar backscattering phases, amplitude, and bond length. The SA samples only feature one major peak at 1.9 Å, whilst the region around 2.6 Å is notably low. This shows the lack of Pt–Pt bonding in the sample and hence the single-atom nature of the Pt. These results are supported via X-ray diffraction (XRD) patterns of the samples (Figure S5), where the NP24 sample shows clear Pt [111, 100] and [110] peaks whilst the SA samples only show peaks related to SWCNTs.

These results show that the K_2PtCl_4 reacts with the SWCNT to form single-atom Pt species, with strong evidence of low valency. No reducing agent was used throughout the process, indicating that electrons from the SWCNT reduce (even partially) the Pt (II) ions, as previously shown.[27] This caused defects and oxygen functionalities to form in the SWCNT, likely forming the binding site of Pt. The Pt donates charge to the SWCNTs, as shown by XPS and XANES, which showed that the lower Pt content SA8 experiences a larger charge transfer. The driving force for this is likely the electron holes formed when the Pt (II) is reduced by electron donation from the SWCNT.

The SACs were tested as catalysts for the hydrogen and air electrodes in acidic conditions. To evaluate the HOR and ORR catalytic activity, they were tested via the FE technique, which enables the precise evaluation of the specific and mass activities. The FE technique is more suitable than the rotating disk electrode (RDE) as it has much higher mass transport and allows measurement of electrocatalyst performance over larger and more realistic potential windows.[28] Table S1 summarizes the details and the FE results of the three different Pt/SWCNT catalysts and one commercial state-of-the-art 30 wt.% Pt/C (TEC10V30E) as a reference. For each catalyst, at least two electrodes were measured under hydrogen (HOR) and oxygen (ORR), and the best-performing linear sweep

26379368, 2024, 1, Downloaded from https://onlinelibrary.wiley.com/doi/10.1002/cey2.409 by Imperial College London, Wiley Online Library on [07/03/2024]. See the Terms and Conditions (https://onlinelibrary.wiley.com/terms-and-conditions) on Wiley Online Library for rules of use; OA articles are governed by the applicable Creative Commons License

voltammograms (LSVs) are plotted in Figure 3A,B. The data are given in terms of mass as no electrochemical surface area (ECSA) could be measured for the catalysts via hydrogen underpotential deposition, whilst CO stripping appeared to vastly underestimate the ECSA resulting in unreliable specific activities (Figure S6 and Table S1). In Figure 3C,D, we extracted the mass activities at selected potentials versus RHE and compared the measured catalysts in a bar chart. Figure 3A,C show that the commercial catalyst has the best HOR activity of 82 A mg_{Pt}^{-1} at 0.05 V versus RHE. While SA8 and SA24 containing single-atom Pt reach 2/3 of that activity at 0.05 V, they have better mass activities than state-of-the-art 30% Pt/C in the high overpotential range (>0.2 V vs. RHE). A similar observation was seen for single-atom Pt-modified covalent triazine frameworks on RDE.[22] As previously reported, a Pt-based catalyst usually shows a double peak feature in the HOR CV like SA8 in Figure 1. The peak at 0.1–0.2 V versus RHE is usually assigned to low-coordination Pt sites and the peak around 0.4 V versus RHE is corresponding to high-coordination Pt sites such as Pt (111).[28] In both SA24 (blue) and NP24 (green), a variety of environments around the HOR active Pt sites blurs out the double feature in the HOR CVs (Figure 3A). The poor activity of NP24 is possibly caused by the blocking of the SWCNT cavities, reducing the transport of hydrogen to Pt.

Figure 3B,D show that state-of-the-art 30% Pt/C has the best ORR activity and its mass activity of 0.27 A mg_{Pt}^{-1} at 0.9 V versus RHE is similar to the literature values on RDE.[30] For all the SWCNT-Pt catalysts, their ORR activities are hugely suppressed in the fuel cell

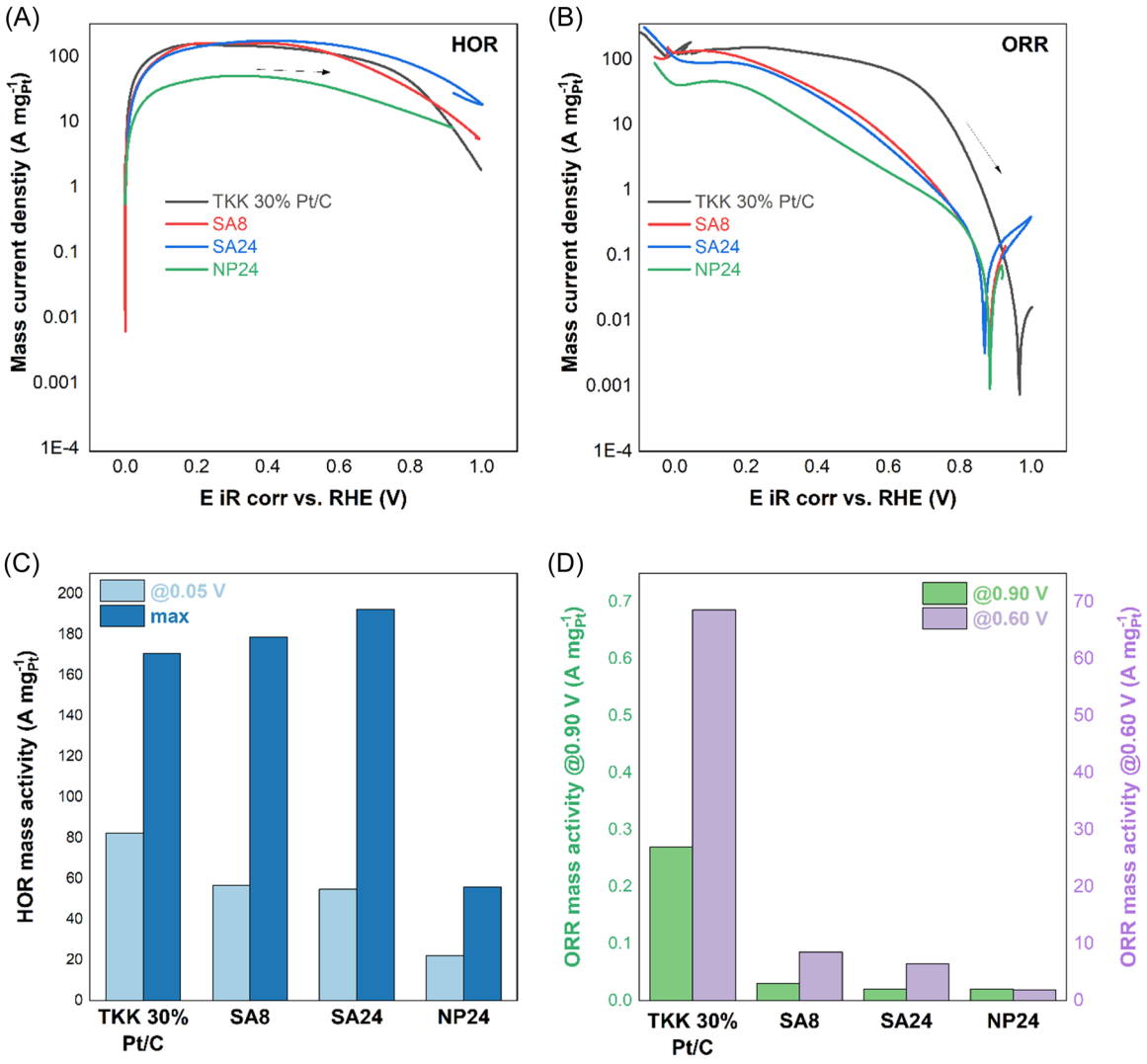


FIGURE 3 LSVs of four different catalysts (state-of-the-art 30% Pt/C, SA8, SA24, and NP24) in 1 M $HClO_4$ at 298 K, 101 kPa, 20 mV s^{-1} (A) under pure hydrogen and (B) under pure oxygen with mass current density plotted in logarithmic scale (inlet in linear scale). (C) The extracted HOR mass activity at 0.05 V versus RHE and the maximum HOR mass activity and (D) the extracted ORR mass activity at 0.9 and 0.6 V versus RHE.

26379368, 2024, 1, Downloaded from https://onlinelibrary.wiley.com/doi/10.1002/cey2.409 by Imperial College London, Wiley Online Library on [07/03/2024]. See the Terms and Conditions (https://onlinelibrary.wiley.com/terms-and-conditions) on Wiley Online Library for rules of use; OA articles are governed by the applicable Creative Commons License

operation potential range (0.4–0.9 V vs. RHE) although the maximum mass activity of SA8 under oxygen overlaps with state-of-the-art 30% Pt/C below 0.1 V versus RHE. Most of the previous studies showed that Pt nanoparticles (>2 nm) supported on carbon prefer a 4-electron oxygen reduction in the low overpotential region (>0.6 V vs. RHE) but gradually become dominated by the 2-electron reduction pathway at higher overpotential (<0.6 V vs. RHE) where more Pt sites are covered by peroxide species.[31] In contrast, the results (Figure 3B) show predominant 2-electron oxygen reduction on SWCNT-Pt catalysts throughout the potential range because Pt grown inside an SWCNT must have a smaller size than the inner diameter (1.6 nm) of the SWCNT and such small Pt particles or single atoms are not good candidates toward the 4-electron ORR.

The stabilities of SA8 and state-of-the-art 30% Pt/C were compared by performing 3000 cycles of the CV under pure oxygen between 0.6 and 1.0 V versus RHE using the FE system (Figure 4A,B). Unsurprisingly, with the increasing number of CVs, the ORR current density decreases. The geometric current density at 0.6 V versus RHE of each cycle was extracted and plotted together with $j/j_{initial}$, and the percentage of initial current density remained, as shown in Figure 4C,D. Although the ORR activity of SA8 is much worse than that of state-of-the-art 30% Pt/C (Figure 1), it remains 35% of the initial performance while Pt/C remains less than 20% (Figure 4C,D). The decay in the current density of state-of-the-art 30% Pt/C is faster than that of SA8, which can come from the difference in 4-electron versus 2-electron ORR mechanism or/and the stability difference of CNT versus VULCAN XC72. XPS and TEM observations were performed on SA8 after 10,000 cycles, which showed the same Pt 4f spectrum (Figure S7) as previously found (single pair of Pt peaks, $4f_{7/2}$ centered at 72.5 eV) and no observable nanoparticles (Figure S8). This shows that the single-atom nature of the catalyst is maintained even after long-term operation.

Overall, the FE provides more information to understand the electrochemical properties of the samples in the large overpotential range. On FEs, SA8 and SA24 showed HOR performance close to the commercial Pt/C. At 0.05 V versus RHE, the HOR mass activity is in the order of SA8 ≈ SA24 > NP24, which shows that for the HOR within the SWCNT, single atoms are vastly superior

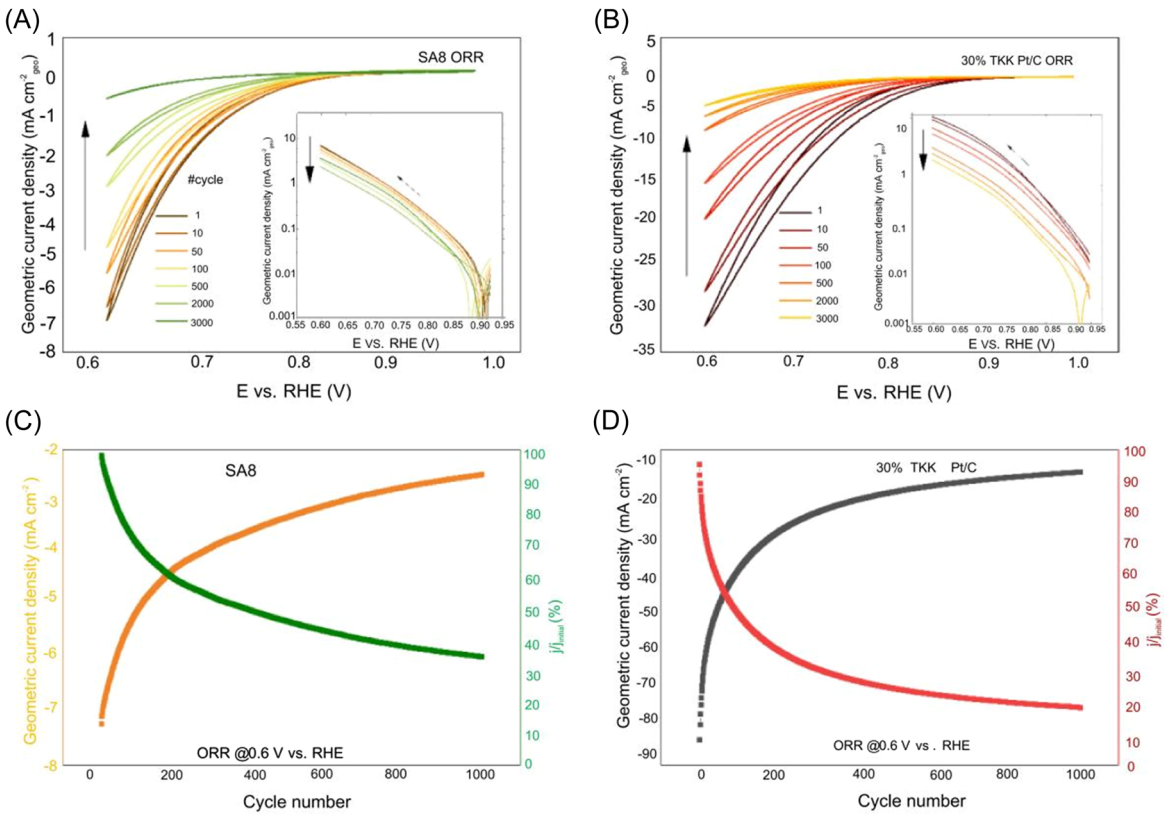


FIGURE 4 Cyclic voltammograms (cycle 1, 10, 50, 100, 500, 2000, 3000) in 1 M $HClO_4$ at 298 K, 101 kPa, 50 mV s^{-1} under pure oxygen of (A) SA8 and (B) state-of-the-art 30% Pt/C. The extracted geometric current density at 0.6 V versus RHE from each stability test cycle (C) of SA8 (orange) with the percentage $j/j_{initial}$ (green) and (D) of state-of-the-art 30% Pt/C (red) with the percentage $j/j_{initial}$ (black).

26379368, 2024, 1, Downloaded from https://onlinelibrary.wiley.com/doi/10.1002/cey2.409 by Imperial College London, Wiley Online Library on [07/03/2024]. See the Terms and Conditions (https://onlinelibrary.wiley.com/terms-and-conditions) on Wiley Online Library for rules of use; OA articles are governed by the applicable Creative Commons License

to the nanoparticles. On the contrary, the SWCNT-encapsulated Pt catalysts are not active in reducing oxygen to water, although they may be useful to selectively produce hydrogen peroxide from oxygen.[32]

Their inactivity toward ORR in the low overpotential range makes the SWCNT-encapsulated Pt materials interesting candidates for PEMFC anode electrocatalysts. Current anode electrocatalysts (Pt nanoparticles on C support) are both highly active toward HOR and ORR. This becomes an issue during start-up when the anode is flooded with air which, when H_2 is introduced, causes the potential at the cathode to increase drastically (to 1.5 V), or shut-down, as O_2 leaks into the anode, causing the same potential rise at the cathode.[33] Alongside the increase in potential, this process also causes heat to be generated. These effects during PEMFC start-up/shutdown give rise to catalyst degradation at both the anode and the cathode.[34] This makes it critical to solve before PEMFCs can be deployed, especially in sectors with intermittent PEMFC usage such as automotive. A catalyst that is insensitive to O_2, as those discussed in this article, would drastically reduce or even eliminate this effect.

4 | CONCLUSION

This work described the synthesis of Pt single-atom electrocatalysts supported inside SWCNTs. STEM, XPS, XRD, and EXAFS results showed the low-valency, single-atom nature of the Pt, whilst XANES and XPS showed a charge transfer from the Pt to the SWCNT. The single-atom samples showed high HOR activity, whilst the sintered NP24 sample showed much lower. The ORR activity of the samples was very low, increasing rapidly at high overpotentials (less than 0.4 V RHE). This showed selectivity toward HOR over ORR and for the 2-electron ORR pathway over the 4-electron pathway. The interaction of the single atoms with hydrogen and oxygen will be investigated to determine the mechanisms behind this strange Pt activity. The single-atom Pt samples have slightly higher HOR activity over a state-of-the-art commercial catalyst whilst being highly insensitive to O_2, making them excellent candidates for PEMFC anode electrocatalysts which avert the known start-up/shutdown issues. This application will be investigated and reported in a future publication.

ACKNOWLEDGMENTS

The authors thank Yaron Kaufmann for the STEM and elemental mapping. We acknowledge Diamond Light Source for time on B18 through the Energy Materials block access group (BAG). SSH acknowledges support from Horizon 2020 program within the ITN Flowcamp. DZ acknowledges funding from the Wohl Foundation for research for the promotion of UK-Israel research cooperation. DZ acknowledges funding from Israel Ministry of Energy (grant #220-11-047).

CONFLICT OF INTEREST STATEMENT

The authors declare that there are no conflicts of interests.

ORCID

Xiaoqian Lin http://orcid.org/0000-0002-1158-6962
David Zitoun http://orcid.org/0000-0003-3383-6165

REFERENCES

1. Yang Y, Peltier CR, Zeng R, et al. Electrocatalysis in alkaline media and alkaline membrane-based energy technologies. *Chem Rev*. 2022;122(6):6117-6321.
2. Sheng W, Gasteiger HA, Shao-Horn Y. Hydrogen oxidation and evolution reaction kinetics on platinum: acid vs alkaline electrolytes. *J Electrochem Soc*. 2010;157(11):B1529.
3. Sheng W, Myint M, Chen JG, Yan Y. Correlating the hydrogen evolution reaction activity in alkaline electrolytes with the hydrogen binding energy on monometallic surfaces. *Energy Environ Sci*. 2013;6(5):1509-1512.
4. Laursen AB, Varela AS, Dionigi F, et al. Electrochemical hydrogen evolution: Sabatiers principle and the volcano plot. *J Chem Educ*. 2012;89(12):1595-1599.
5. Cruz-Martínez H, Rojas-Chávez H, Matadamas-Ortiz PT, et al. Current progress of Pt-based ORR electrocatalysts for PEMFCs: an integrated view combining theory and experiment. *Mater Today Phys*. 2021;19:100406.
6. Li L, Wang P, Shao Q, Huang X. Recent progress in advanced electrocatalyst design for acidic oxygen evolution reaction. *Adv Mater*. 2021;33(50):2004243.
7. Greenwood NN, Earnshaw ABT. *Chemistry of Elements*. 2nd ed., Elsevier; 1997:1144-1172.
8. Huang J, Li Z, Zhang J. Review of characterization and modeling of polymer electrolyte fuel cell catalyst layer: the blessing and curse of ionomer. *Front Energy*. 2017;11(3):334-364.
9. Unni SM, Dhavale VM, Pillai VK, Kurungot S. High Pt utilization electrodes for polymer electrolyte membrane fuel cells by dispersing Pt particles formed by a preprecipitation method on carbon "polished" with polypyrrole. *J Phys Chem C*. 2010;114(34):14654-14661.
10. Vielstich W, Lamm A, Gasteiger HA, Yokokawa H. *Handbook of Fuel Cells. Fundamentals, Technology, Applications*. John Wiley & Sons, Ltd; 2009.
11. Liu J, Jiao M, Lu L, et al. High performance platinum single atom electrocatalyst for oxygen reduction reaction. *Nat Commun*. 2017;8:15938.
12. Qiao B, Wang A, Yang X, et al. Single-atom catalysis of CO oxidation using $Pt1/FeO_x$. *Nat Chem*. 2011;3(8):634-641.
13. Kaiser SK, Chen Z, Faust Akl D, Mitchell S, Pérez-Ramírez J. Single-atom catalysts across the periodic table. *Chem Rev*. 2020;120(21):11703-11809.
14. Jones J, Xiong H, DeLaRiva AT, et al. Thermally stable single-atom platinum-on-ceria catalysts via atom trapping. *Science*. 2016;353(6295):150-154.

26379368, 2024, 1, Downloaded from https://onlinelibrary.wiley.com/doi/10.1002/cey2.409 by Imperial College London, Wiley Online Library on [07/03/2024]. See the Terms and Conditions (https://onlinelibrary.wiley.com/terms-and-conditions) on Wiley Online Library for rules of use; OA articles are governed by the applicable Creative Commons License

15. Chang TY, Tanaka Y, Ishikawa R, et al. Direct imaging of Pt single atoms adsorbed on TiO_2 (110) surfaces. *Nano Lett*. 2014;14(1):134-138.
16. Thang HV, Pacchioni G, DeRita L, Christopher P. Nature of stable single atom Pt catalysts dispersed on anatase TiO_2. *J Catal*. 2018;367:104-114.
17. Sun S, Zhang G, Gauquelin N, et al. Single-atom catalysis using Pt/graphene achieved through atomic layer deposition. *Sci Rep*. 2013;3(1):1775.
18. Shi Z, Yang W, Gu Y, Liao T, Sun Z. Metal-nitrogen-doped carbon materials as highly efficient catalysts: progress and rational design. *Adv Sci*. 2020;7(15):2001069.
19. Zhang J, Zhao Y, Guo X, et al. Single platinum atoms immobilized on an MXene as an efficient catalyst for the hydrogen evolution reaction. *Nat Catal*. 2018;1(12):985-992.
20. Zhong W, Tu W, Wang Z, et al. Ultralow-temperature assisted synthesis of single platinum atoms anchored on carbon nanotubes for efficiently electrocatalytic acidic hydrogen evolution. *J Energy Chem*. 2020;51:280-284.
21. Zhu C, Fu S, Shi Q, Du D, Lin Y. Single-atom electrocatalysts. *Angew Chem Int Ed*. 2017;56(45):13944-13960.
22. Kamai R, Kamiya K, Hashimoto K, Nakanishi S. Oxygen-tolerant electrodes with platinum-loaded covalent triazine frameworks for the hydrogen oxidation reaction. *Angew Chem Int Ed*. 2016;55(42):13184-13188.
23. Lin X, Zalitis CM, Sharman J, et al. Correction to "electrocatalyst performance at the gas/electrolyte interface under high mass transport conditions: optimization of the 'floating electrode' method". *ACS Appl Mater Interfaces*. 2020;12(51):57667.
24. Hardisty SS, Saadi K, Nagaprasad Reddy S, Grinberg I, Zitoun D. Ionically selective carbon nanotubes for hydrogen electrocatalysis in the hydrogen–bromine redox flow battery. *Mater Today Energy*. 2022;24:100937.
25. Bayindir Z, Duchesne PN, Cook SC, MacDonald MA, Zhang P. X-ray spectroscopy studies on the surface structural characteristics and electronic properties of platinum nanoparticles. *J Chem Phys*. 2009;131(24):244716.
26. Zhou KL, Wang Z, Han CB, et al. Platinum single-atom catalyst coupled with transition metal/metal oxide heterostructure for accelerating alkaline hydrogen evolution reaction. *Nat Commun*. 2021;12:3783.
27. Choi HC, Shim M, Bangsaruntip S, Dai H. Spontaneous reduction of metal ions on the sidewalls of carbon nanotubes. *J Am Chem Soc*. 2002;124(31):9058-9059.
28. Zalitis CM, Kramer D, Kucernak AR. Electrocatalytic performance of fuel cell reactions at low catalyst loading and high mass transport. *Phys Chem Chem Phys*. 2013;15(12):4329-4340.
29. Zalitis CM, Kucernak AR, Sharman J, Wright E. Design principles for platinum nanoparticles catalysing electrochemical hydrogen evolution and oxidation reactions: edges are much more active than facets. *J Mater Chem A*. 2017;5(44):23328-23338.
30. Gasteiger HA, Kocha SS, Sompalli B, Wagner FT. Activity benchmarks and requirements for Pt, Pt-alloy, and non-Pt oxygen reduction catalysts for PEMFCs. *Appl Catal B*. 2005;56(1-2):9-35.
31. Markiewicz M, Zalitis C, Kucernak A. Performance measurements and modelling of the ORR on fuel cell electrocatalysts—the modified double trap model. *Electrochim Acta*. 2015;179:126-136.
32. Wang N, Ma S, Zuo P, Duan J, Hou B. Recent progress of electrochemical production of hydrogen peroxide by two-electron oxygen reduction reaction. *Adv Sci*. 2021;8(15):2100076.
33. Reiser CA, Bregoli L, Patterson TW, et al. A reverse-current decay mechanism for fuel cells. *Electrochem Solid-State Lett*. 2005;8(6):A273.
34. Yu Y, Li H, Wang H, Yuan XZ, Wang G, Pan M. A review on performance degradation of proton exchange membrane fuel cells during startup and shutdown processes: causes, consequences, and mitigation strategies. *J Power Sources*. 2012;205:10-23.

SUPPORTING INFORMATION

Additional supporting information can be found online in the Supporting Information section at the end of this article.

How to cite this article: Hardisty SS, Lin X, Kucernak ARJ, Zitoun D. Single-atom Pt on carbon nanotubes for selective electrocatalysis. *Carbon Energy*. 2024;6:e409. doi:10.1002/cey2.409

26379368, 2024, 1, Downloaded from https://onlinelibrary.wiley.com/doi/10.1002/cey2.409 by Imperial College London, Wiley Online Library on [07/03/2024]. See the Terms and Conditions (https://onlinelibrary.wiley.com/terms-and-conditions) on Wiley Online Library for rules of use; OA articles are governed by the applicable Creative Commons License